Meteoritics & Planetary Science 39, Nr 8, 1321–1341 (2004)
Abstract available online at http://meteoritics.org

Thuathe, a new H4/5 chondrite from Lesotho: History of the fall, petrography, and geochemistry

W. U. REIMOLD,[1*] P. C. BUCHANAN,[2] D. AMBROSE,[3] C. KOEBERL,[4] I. FRANCHI,[5] C. LALKHAN,[6] L. SCHULTZ,[7] L. FRANKE,[7] and G. HEUSSER[8]

[1]Impact Cratering Research Group, School of Geosciences, University of the Witwatersrand, Private Bag 3, P.O. Wits 2050, Johannesburg, South Africa
[2]Antarctic Meteorite Research Center, National Institute for Polar Research, 1–9–10 Kaga, Itabashi-ku, Tokyo 173–8515, Japan
[3]Institute of Education, National University of Lesotho, Roma 180, Lesotho
[4]Department of Geological Sciences, University of Vienna, Althanstr. 14, A-1090 Vienna, Austria
[5]Planetary and Space Science Research Institute, Open University, Milton Keynes MK7 6AA, UK
[6]Electron Microscope Unit, University of the Witwatersrand, Private Bag 3, P.O. Wits 2050, Johannesburg, South Africa
[7]Max-Planck-Institute for Chemistry, Cosmochemistry Division, P.O. Box 3060, D-55020 Mainz, Germany
[8]Max-Planck-Institute for Nuclear Physics, P.O. Box 103 980, D-69029 Heidelberg, Germany
*Corresponding author. E-mail: reimoldw@geosciences.wits.ac.za

(Received 22 October 2003; revision accepted 7 April 2004)

Abstract–On July 21, 2002, a meteorite fall occurred over the Thuathe plateau of western Lesotho. The well-defined strewn field covers an area of 1.9 × 7.4 km. Many of the recovered specimens display a brecciated texture with leucocratic, angular to subrounded clasts in a somewhat darker groundmass. Mineralogical and chemical data, as well as oxygen isotopic analysis, indicate that Thuathe is an H4/5, S2/3 meteorite, with local H3 or H6 character. A number of anomalous features include somewhat high Co contents of kamacite and taenite relative to normal H-group chondrites. Oxygen isotopic data plot at the edge of the normal H chondrite data field. Variable contents of metallic mineral phases and troilite result in a heterogeneous bulk composition (e.g., with regard to Si, Fe, and Mg), resulting in a spread of major element ratios that is not consistent with previously accepted H-group composition. Trace element abundances are generally consistent with H chondritic composition, and Kr and Xe isotopic data agree with an H4 classification for this meteorite. Noble gas analysis gave U, Th-^{4}He gas retention and K-Ar ages typical for H chondrites; no major thermal event affected this material since ~3.7 Ga. The exposure age for Thuathe is 5 Ma, somewhat lower than for other H chondrites. Cosmogenic nuclide analysis indicates a pre-atmospheric radius of this meteorite between 35 and 40 cm. In the absence of evidence for solar gases, we classify Thuathe as a fragmental breccia.

Numerous narrow, black veins cut across samples of Thuathe and are the result of a brittle deformation event that also caused local melting, especially in portions rich in sulfide. The formation of these veinlets is not the result of locally enhanced shock pressures (i.e., of shock melting) but rather of shearing under brittle conditions with local, friction-related temperature excursions causing melting mostly of Fe-sulfide and FeNi-metal but also, locally, of silicate minerals. Frictional temperature excursions must have attained values in excess of 1500 °C to permit complete melting of forsteritic olivine.

INTRODUCTION

At 15:47 local time (13:47 GMT) on July 21, 2002, a large meteorite fell over the western Thuathe plateau (Fig. 1a; locally known as Berea plateau), some 9 km east of Maseru in Lesotho, southern Africa (Figs. 1a and 1b). A loud noise was heard by inhabitants of this region for about 15 sec; initial reports of noise and sightings quickly established that this event represented the entry of a meteoroid into the atmosphere, that this projectile travelled in an approximate east-west direction, and that a number of stones had fallen in and around the small village of Ha Ralimo. During the weeks after the event, the region where the noise was heard was delineated (Fig. 1b). The circle of ~100 km radius on this figure illustrates the region within which the noise was sufficiently distinct to be clearly remembered by witnesses.

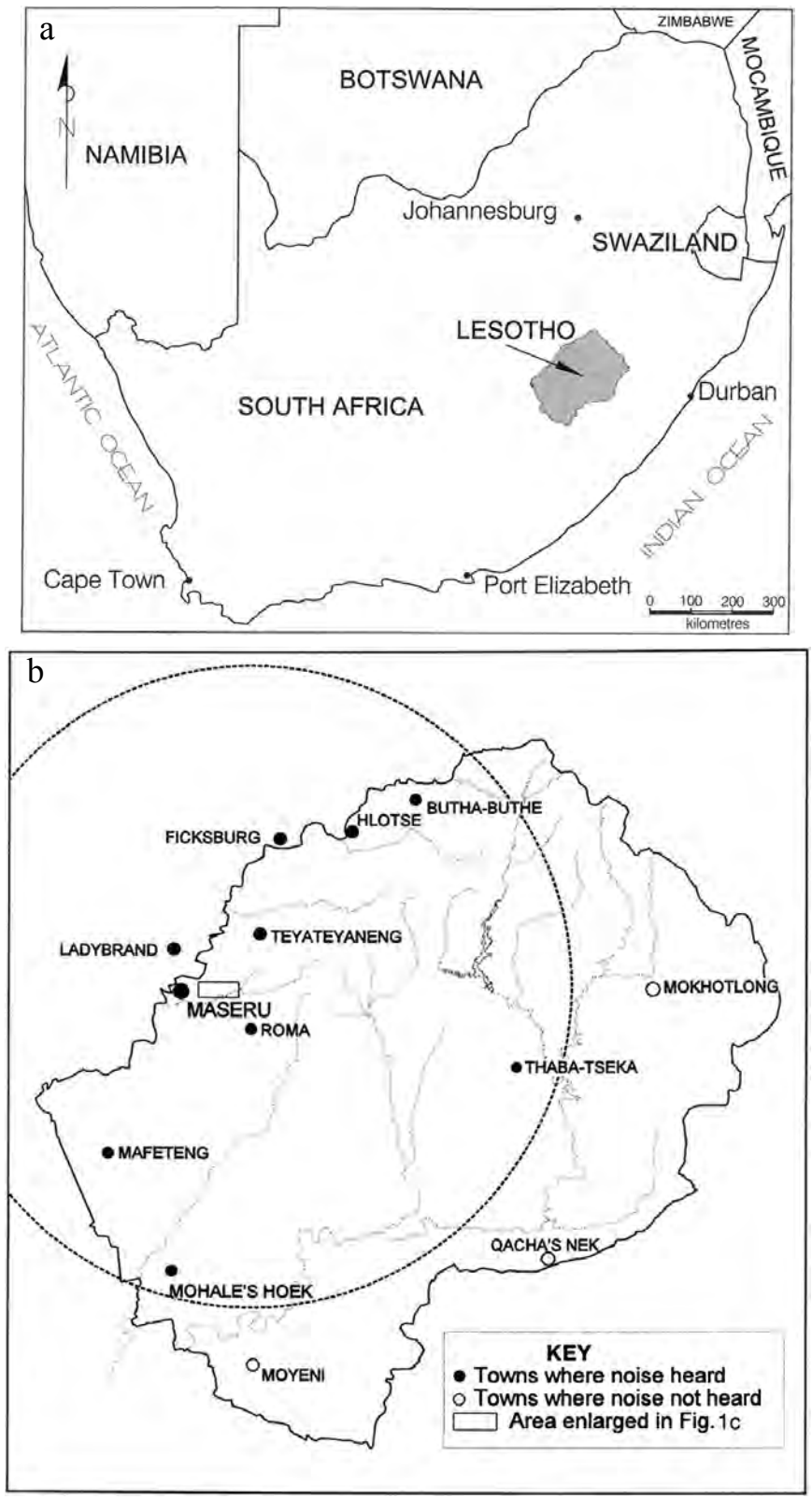

Fig. 1. a) Map of southern Africa with location of Lesotho. The Thuathe fall occurred just east of the capital Maseru; b) region of Lesotho and southern Free State Province (South Africa), where the noise accompanying the fall of the Thuathe meteorite was heard (indicated by the 200 km-diameter circle).

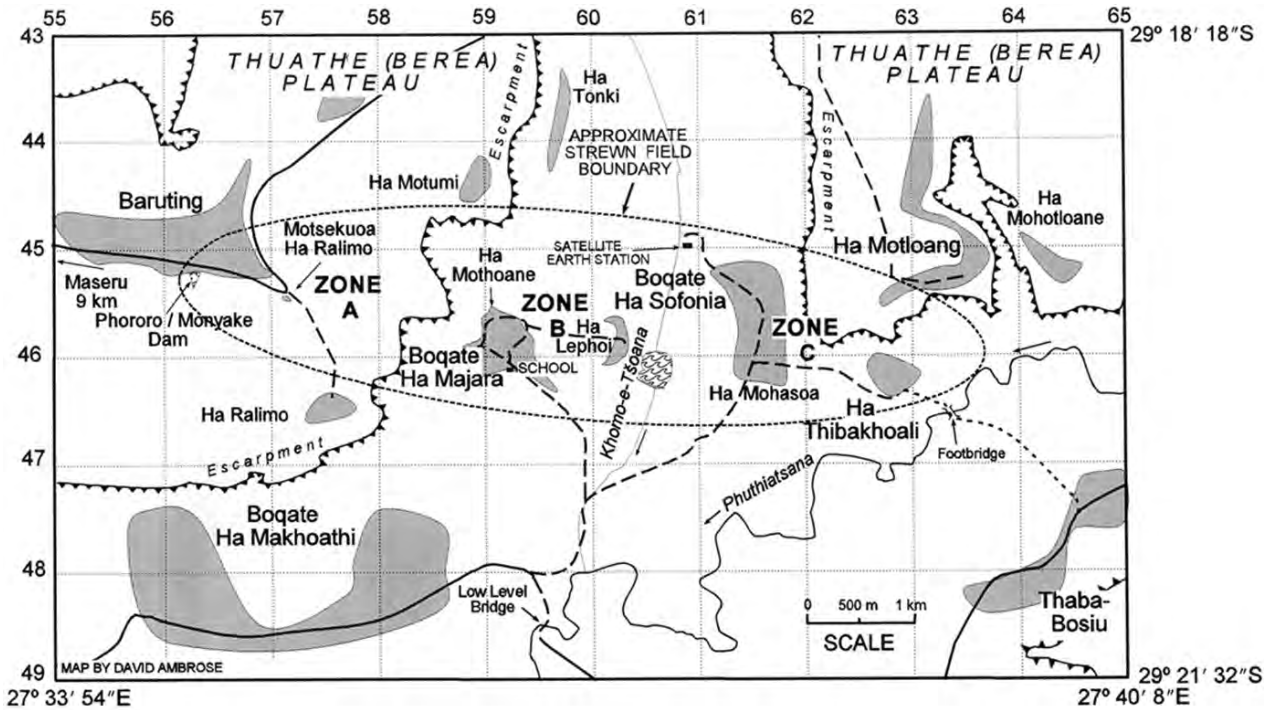

Fig. 1. *Continued.* c) Map of the Thuathe strewn field, based on the local 1:50,000 topographic map. Tarred roads = thin, continuous lines; streams = very thin continuous lines. Shaded areas = villages and hamlets. Two dams are shown by wavy patterns. The grid numbers refer to the South African Lo 27° survey grid system.

Dozens of eyewitness reports also rapidly confirmed the direction of movement of the bolide and the area over which a large number of stones had fallen (Fig. 1c). Detailed accounts of this early investigative phase were published by Ambrose and Talukdar (2003), Ambrose et al. (2003), Lombard et al. (2003), and McKenzie (2003).

Preliminary chemical and mineralogical classification of this new fall was presented by Ambrose et al. (2003), Lombard et al. (2003), and Reimold et al. (2003). The Meteorite Nomenclature Committee of the Meteoritical Society officially approved the name Thuathe for this new meteorite (Russell et al. 2003). Thuathe is, to our knowledge, the first meteorite recovered from the country of Lesotho.

CONSIDERATIONS REGARDING THE TIMING AND DIRECTION OF THE THUATHE FALL

The timing of the fall was recorded at Roma (Lesotho) as 15:49 (13:49 GMT), with a possible error of ±1 min; the sound duration was recorded as 15 ± 5 sec. The location of this observation is 16 km from the center of the strewn field on a bearing of 143°. Allowance must be made for the speed of sound. If the origin of the sound was at a height of 40 km above the center of the strewn field, it would have taken ~2 min for the sound to reach Roma. This indicates that the actual time of the meteoroid explosion was 13:47 GMT, ±1 min.

Early observations suggested that the meteoroid travelled in a direct east-west path. The orientation of the strewn field (next section) confirms this but provides additional refinement, indicating that the movement was on a bearing of 275° (estimated error: 3°). The angle at which the meteoroid entered the atmosphere and the height at which it exploded can be estimated based on eyewitness reports: the explosion height was variably estimated at 151 to 84 km, or at 66 to 40 km; most estimates scatter around 60 km high.

THE EXTENT OF THE STREWN FIELD

A number of residents of the western Thuathe plateau had narrow escapes when stones "rained down" on them or their dwellings; however, not a single person seems to have been injured. Damage to property was also minimal. The strewn field was initially thought to be centered on Ha Ralimo, but by early 2003, it was established that the area covered by this fall was ~7.4 km long and 1.9 km wide (Fig. 1c). This roughly elliptical area has these coordinates: major axis: between 29°19′31″S/27°34′37″E and 29°19′54″S/27°39′19″E; minor axis: between 29°19′11″S/27°37′02″E and 29°20′14″S/27°36′54″E. This area straddles the Thuathe plateau escarpment. The plateau is elevated by about 1850 m above mean sea level and is bounded by a steep escarpment formed by Clarens Formation sandstone cliffs. The strewn field shown in Fig. 1c covers three different zones, from west to east: zone A on top of the plateau is bounded to the west by the escarpment, zone B covers the area between the escarpment and the Khomo-e-Tšoana

stream, and zone C covers the area to the east of the stream (Fig. 1c). Zone C is mainly lowland but also contains a small part of the eastern lobe of the plateau. The greatest density of stones was found close to the escarpment, north and northwest of the village of Ha Ralimo (zone A) and between the Letsatseng dyke (between the villages of Ha Mothoane and Ha Tonki) and a rock pinnacle known as 'Mamolalana, just off the escarpment near the village of Boqate Ha Majara (western part of zone B; Fig. 1c). The recovered stones range in mass from ~3.5 kg to less than a gram. In addition, a "large" stone may have fallen into the water reservoir behind the Phororo/Monyake Dam close to the western end of the strewn field. The largest stone found to date (about 3.5 kg) made a small hole, and we estimate that the specimen was retrieved from soil from no more than 40 cm deep.

From the dimensions of the strewn field, the meteoroid apparently had a low angle of approach; a first approximation is suggested by arc cos (1.9/7.4) = 75° (angle to the vertical). The strewn field is located in a relatively high rainfall region. Winter is, however, the dry season when frost occurs most nights and rain is rare; snow falls are recorded in some winters. For 27 days before the fall, there had been no precipitation. Nor was there precipitation in the following 25 days. Consequently the ground, typically open grassland and fallow fields, was relatively hard and mainly devoid of vegetation, facilitating recovery of stones. Heavy rain did, however, fall thereafter, and many stones recovered after that time show some oxidation.

STONE STATISTICS

By November 2002, 418 stones of different sizes had been collected by D. Ambrose and collaborators (Ambrose et al. 2003). Some 30 other specimens had been collected by Free State University personnel and students (A. Lombard, personal communication); for these samples, no mass statistics are available to us. Since then, Thuathe collectors' fever has become rampant throughout the world, and not only have the Lesotho-based collectors obtained many more specimens, but meteorite dealers and collectors from around the world have repeatedly visited the Thuathe plateau. It does not seem unlikely that perhaps 60 kg have been recovered altogether.

The latest statistics available to us include data for 1034 cataloged (Ambrose 2003) fragments. These fragments correspond to 1029 stones, as the remaining five fragments could be paired and were found to have been broken apart by locals. This may also, in all likelihood, be the case for several other fragments that have been cataloged separately. The 1034 pieces have a total mass of 45.3 kg, with a mean mass for this collection of 44.1 g—significantly less than the mean mass of 66.1 g reported by Ambrose et al. (2003). Clearly, with time, the average mass of new finds has decreased. Table 1a illustrates the statistical distribution of stone masses, with five stones known to be over 1 kg (including one large stone held in private hands; not including the stone in the dam). Considering that the area, which is mostly covered by hard soil and thin grass vegetation, has been well-"combed" for fragments and that stones did not embed themselves deeply into the soil, and as the cultivated parts of this area were largely unploughed at the time of the fall, it is considered highly unlikely that many more stones of more than 1 kg mass remain to be collected. As the size diminishes, the number recovered must be proportionately less, and we estimate that perhaps as little as 50% of stones between 100 g and 1 kg have been recovered to date, 10% of those between 10 and 100 g, and perhaps as little as 1% of those between 1 and 10 g. If these first order figures are only roughly accurate, they indicate that a total mass of ~350 kg in the form of fragments >1 g could have fallen.

DISTRIBUTION OF STONES RECOVERED FROM THE DIFFERENT ZONES OF THE STREWN FIELD

The masses of stones and mean masses of stones recovered from the three naturally defined zones of the strewn field are shown in Table 1b. Most of the stones were recovered from the westernmost zone A (Fig. 1c). With respect to the mean mass per zone, there is little difference between the values for zones A and B, but that for zone C is considerably less. This could be viewed as a result of the strenuous efforts by local people to find more—but only very small—stones in response to the establishment of a "Meteorite Fund" for the upgrading of a local, communal structure from proceeds of early meteorite sales in zone C. However, the lower mean value for zone C is also influenced by the fact that no relatively large stones have been obtained from that area (Table 1c). Table 1c compares the actual distribution of stones derived from the three zones. Zone A is the smallest area but had, by far, the largest number of stones. In fact, the density of stones that were recovered from zone A (about 250 per km^2) is >6 times the densities of stones that fell in zones B and C. Within a given zone, densities are also not uniform. A plot using the grid references for zone B stones (not reproduced here) shows that many more stones were found close to the escarpment on the west side of zone B. It is thought that this reflects not only the increasing density of stones from east to west (Table 1c), but that an additional effect results from the relatively low angle of approach of falling stones that may have been as low as 15° to the horizontal, based on the ratio of lengths for the major axes of the strewn field. This could have led to many stones bouncing off the nearly vertical cliff face. The largest stones (those >~700 g) were all found in the westernmost zone A. Several specimens of intermediate size (about 300 to 700 g) were, however, collected in zone B. The largest stone found in zone C has a mass of only 121 g. These observations are in excellent agreement with findings at other strewn fields (e.g., Bevan and De Laeter 2002), i.e., that larger

Table 1a. Distribution of stone masses.

	>1 kg	100 g–1 kg	10–100 g	1–10 g	Total #
No. specs.	4	82	599	344	1029

Table 1b. Masses of cataloged stones per geographic zone.

	Zone A stones			Zone B stones			Zone C stones			Total stones		
	No.	Total mass	Mean mass	No.	Total mass	Mean mass	No.	Total mass	Mean mass	No.	Total mass	Mean mass
Total	730	34311	47	161	9072	56.3	138	1954	14.2	1029	45337	44.1

Table 1c. Comparison of areal densities of stones in the different zones.

Zone	Area (km^2)	No. of stones	Areal density (stones per km^2)	Total mass (g)	Mean mass (g)	Mass (g) per km^2	Smallest stone (g)	Largest stone (g)
A	2.94	730	248.3	34311	47	11670.4	1	3147
B	4.08	161	39.5	9072	56.3	2223.5	2	685
C	4.02	138	34.3	1954	14.2	486.1	1	121
A + B + C	11.04	1029	93.1	45337	44.1	4106.6	1	2387

pieces generally travel further than smaller fragments because of their greater momentum.

MACROSCOPIC CHARACTERISTICS OF METEORITE FRAGMENTS

Many stones have angular shapes, and the presence of fusion crust on many angular faces shows that these geometries are the result of fragmentation in the atmosphere. Fusion crust is typically only 0.1 mm thick on stones in zone A but tends to be slightly thicker on some pieces from further to the east, up to 0.2 mm thickness or more on some stones from zone C. Variable thickness of fusion crust has been noted on some specimens (McKenzie 2003) and is considered the result of in-flight fragmentation. Many fragments reveal six or more, apparently successively formed, fractures. The earliest fractures are well-fused and smoothed out. Later-formed fractures may indicate that they were heated, with earlier fusion melt "bleeding" over the edge or streaking across a surface. Finally, there are fresh fractures devoid of any evidence of heating, and it is known that at least some of these represent fractures related to the final impact or to human manipulation of fragments. On such fresh fracture surfaces, the meteorite interior has variably grey color with rare indications of brecciation (see below). Figure 2 shows a stone that clearly displays a relatively more leucocratic component set into zones of darker material and that is entirely covered with a network of streaks of fused material. A few specimens contain up to 35 vol% dark lithology. Small (<1 to 2 mm) chondrules are readily distinguished, and most surfaces display ample specks of metallic phases. Very thin (<1 mm) black veinlets can also be discerned on the surfaces of some broken samples and resemble the so-called "shock veins" known from many ordinary chondrites. Stones that were retrieved after several weeks or more show brownish, rusty staining on fracture surfaces. On larger stones, regmaglypts are common.

MINERALOGY

Twelve polished thin sections were prepared from six Thuathe specimens (Nos 55, 58, 59, 60, 61, 193). They were studied by optical microscopy, electron microprobe analysis (EMPA), and scanning electron microscopy (SEM). Mineral compositions were determined using the JEOL JXA-8800M Superprobe at the National Institute of Polar Research in Tokyo, Japan, operated at 15 kV and 20 nA. Counting times were 30 sec for most elements. The following standards were used: for metal and sulfide, Ni, Cu, Co, Fe, and Mn metal standards as well as ZnS and PbS standards; for the silicate analyses, albite, spessartite, orthoclase, olivine, chromite, apatite, and wollastonite standards were used, as well as TiO_2, SiO_2, MgO, Fe_2O_3, and Al_2O_3 oxide standards. ZAF corrections were made by application of the JEOL online programs. SEM was conducted at the University of the Witwatersrand's Electron Microscopy Unit, where a JEOL JSM-840 instrument is equipped with a Link AN-10 000 energy-dispersive X-ray spectrometer, as well as at the Microanalytical Facility of the University of Pretoria, with a JSM-5800LS instrument. All observations and analyses were done at 20 kV acceleration potential and 20 nA sample current.

Modal Compositions

Figure 3a displays the typical dense packing of chondrules and chondrule fragments, with a large proportion of metal. The dark material in Fig. 3b not only represents metal/sulfide phases, but also the nearly opaque groundmass. SEM images of this material are shown in Figs. 3f and 3g. The feldspathic matrix to this dark component was analyzed by SEM-EDX to be rich in Ca and also to contain minor and variable K contents (on a several μm scale). Figure 3h illustrates that, in places, the feldspathic groundmass is also fractured or brecciated. This groundmass, locally, can also

Fig. 2. Stone 267 (Ambrose 2003; 99 g; ~60 × 40 × 30 mm) comprises a leucocratic component and a somewhat darker phase (prominent in the uppermost part), both of which are criss-crossed by streaks of melt (fusion crust). The irregular distribution of this melt demonstrates that this sample tumbled through the atmosphere.

contain additional phases, including chromite (Fig. 3i), troilite, or FeNi metal. The groundmass in the lighter component is often clearly defined and occurs only as narrow seams surrounding chondrules and other well-defined units (such as metal blebs or large olivine fragments). Figure 3c not only shows a variety of chondrules (such as a compound chondrule in the upper right portion of this image) in the light component, but also the fractured and brecciated nature of a large chondrule. Deformation is pervasive in both types of material (light and dark), as shown in both Figs. 3a and 3b, where black breccia veins are also prominent. Modal compositions determined by point counting are quite variable (Table 2). All samples have a large proportion of chondrules (35 to >60 vol%). Metallic phases are abundant and, in some samples, may exceed 45 vol%, but generally are of the order of 20–30 vol%. The narrow black veinlets are distinct in thin sections as well. SEM analysis showed that they are even more abundant than obvious on fresh fracture surfaces. In thin sections, angular patches of melt have been identified, with abundant droplets of melted metal or obvious cataclasis of minerals (Figs 3c and 3d). They indicate the presence of many veinlets oblique or perpendicular to the thin section planes.

The major minerals in Thuathe are olivine, FeNi-metal, and troilite (Table 2). Minor orthopyroxene and traces of pigeonite, clinopyroxene (augite), chromite, and Ca-phosphate have been detected as well. Plagioclase rarely occurs as sizable grains (>50 μm), but is ubiquitous as a component of the groundmass, more abundant in the dark than in the leucocratic component. Chondrules contain a feldspathic groundmass that is completely devitrified (micro-crystalline). Chromite and Ca-phosphate crystals of up to >50 μm size have been observed but predominantly occur as <10-μm-sized particles.

The modal compositions of dark and light phases are not significantly different (Table 2), but the dark phase has a higher proportion of near-opaque groundmass. In addition, the dark phase has the generally finer grain size of much of the metal-sulfide material, and evidence of brecciation is ubiquitous in this phase. The abundance of chondrules and possibly chondrule-derived fragments of olivine and orthopyroxene does not vary much between the light and dark zones. In both materials, chondrule outlines are distinct and well-preserved. Part of the alteration effects (rusting) observed at the thin section scale must be considered the result of sample preparation, as the sections were prepared from interior portions of samples, at least 1 cm from original sample surfaces. However, most samples display narrow (<15 μm) veinlets of a low reflective phase, which was analyzed by SEM-EDX to consist of mostly iron with a very minor amount of nickel (Fe:Ni = >20:1). No lateral displacements have been noted along these veins, which are, in turn, cut and locally displaced by the narrow deformation veins discussed below. Thus, it appears that these grey

Table 2. Modal analyses of two Thuathe samples (# 58, #61B-1), as well as of two splits (light and dark component, respectively) of a second slice from specimen #61B.

Mineral	#58	#61B-1	#61B Dark	#61B Light
FeNi metal	25.5	17.9	10.4	10.5
Troilite	18.8	11	11.8	7.6
Groundmass	13.5	12.1	18.3	12.9
Chondrules	35.1	50.1	52	63.1
Large olivine xx	4.2	7	5.7	4.9
Melt/Catacl. Veining/pods	1.7	1.1	1.1	0
Large plagioclase xx	0.1	0	0	0
Large opx xx	0.1	0.5	0	0.3
Chromite	0.8	0.3	0.7	0.7
Ca-phosphate	0.1	0	0.1	0
Total	99.9	100	100.1	100

veinlets represent a relatively early stage of deformation and/or alteration.

Chondrules

Chondrules are generally quite densely packed (Figs. 3a, 3b, and 3e), with only narrow rimming by groundmass. The majority of chondrules are rounded to sub-rounded, but ovoid and droplet shapes also occur. A wide variety of chondrule types is present, including cryptocrystalline (feldspathic groundmass-rich), radial pyroxene, radial olivine, barred olivine, porphyritic olivine, rare porphyritic pyroxene, and compound chondrule types. This latter group includes such diverse combinations as barred/porphyritic, barred/granulitic and porphyritic/granulitic types.

Metal and Sulfide Phases

FeNi metal (kamacite >> taenite) and sulfide in Thuathe have a wide variety of textures. Figure 4a shows disseminated FeNi metal and minor troilite in a wide range of grain sizes and interrelationships. Individual metal and sulfide grains may occur in euhedral crystal shapes; more commonly, irregular blebs are observed. Sulfide particles may occur individually or in association with FeNi metal—either showing apparent exsolution or being "smeared out" between FeNi metal layers as a result of obvious shearing. Grain sizes of FeNi metal and troilite particles range from >1.5 mm to <20 μm. Figure 4b illustrates some metallic/sulfide particles that are the result of recrystallization that caused the formation of spongy textures with the metal/sulfide minerals enclosing small areas of silicate (also Figs. 4c and 4d). Figure 4e shows a large, irregularly shaped troilite grain with an attachment of a mixed sulfide/FeNi metal particle in close textural relationship. Such texture is frequently observed along deformation veins where sulfide has been physically incorporated between FeNi metal due to shearing. Troilite and chromite also occur in another textural association (compare Fig. 3j). Trails of tiny blebs of these minerals have been observed by SEM in olivine crystals, in both planar and irregular alignments. Whether these trails represent magmatic exsolution or are the result of local shock melting is debatable.

Mineral Chemistry

Olivine and pyroxene compositions are listed in Table 3. Olivine compositions (Fig. 5a) are well-equilibrated, with an average composition (108 analyses) of $Fa_{17.1 \pm 0.8}$ mol% (1σ standard deviation). This includes analyses of olivine in the dark and light phases, in chondrules, and in groundmass. Orthopyroxene (94 analyses) is also well-equilibrated, with an average composition of $Wo_{0.96}En_{83.6}Fs_{15.5}$ and 1σ standard deviations of 0.22, 1.1, and 1.1 mol%, respectively. Only a few augite compositions (Table 3; Fig. 5a) were obtained. In Table 4, average EMPA analyses for kamacite, taenite, and troilite are compiled and illustrate that the compositions of these minerals are also well-constrained. Few plagioclase compositions were determined, but a large number of semi-quantitative SEM-EDX analyses show that this mineral phase is also of constant composition, with a strong albite component but somewhat variable amounts of K.

In a plot of mol% Fs in low-Ca pyroxene versus mol% Fa in olivine from H, L, and LL chondrites (Fig. 5b), Thuathe mineral compositions plot exactly into the cluster of data from H chondrites (see also Rubin 1990). Minor element abundances in olivine and orthopyroxene of Thuathe are also in good agreement with data for H chondrites of types 4 and 5 (Figs. 5c and 5d). The Ni contents of Thuathe kamacite and taenite are also comparable to those in H chondrite FeNi-metal, although this parameter does not separate H and L chondrite groups entirely (Fig. 6; Rubin 1990). The abundance of Co in Thuathe FeNi-metal was determined as distinctly higher than in H chondrites and rather comparable to that of L chondrites (Figs. 6b–6d; also after Rubin 1990). We carefully examined the possibility that this "excess" Co could be the result of an analytical artefact (overlay of FeKβ on the CoKα line), but the maximum contribution that could be related to this effect is 0.15 wt%. Correction for this would bring Thuathe data into the upper range of Co abundance in H chondrite kamacite (Fig. 6b).

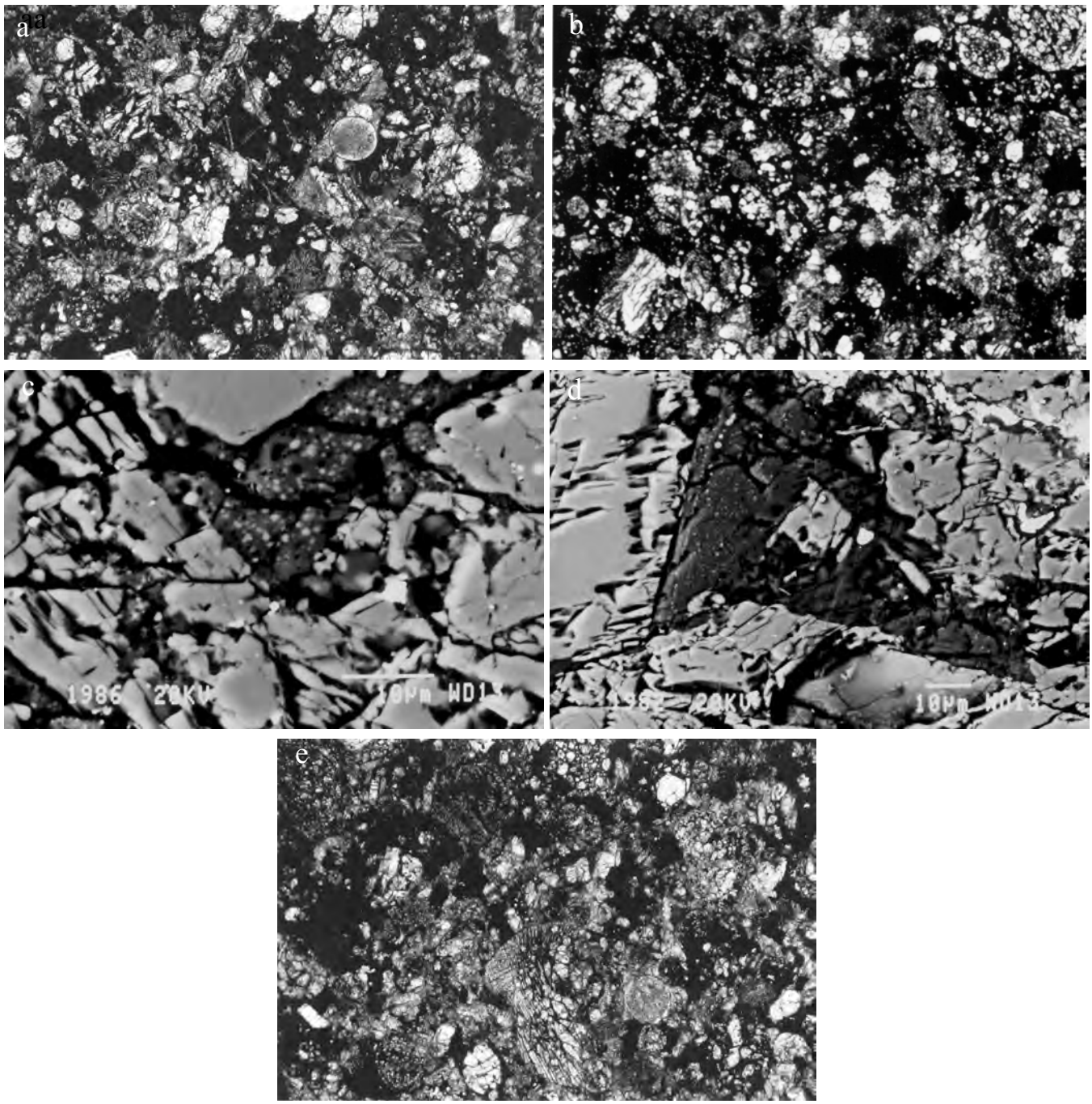

Fig. 3. Optical microscopic and SEM images taken on thin sections of sample #61: a) dense packing of chondrules and chondrule fragments in light component. Dark patches represent metal and sulfide blebs, while dark groundmass is limited to narrow seams around larger units. The area shown is transected by a black vein that obviously displaces a dark chondrule. Width of field of view: 5.5 mm, plane polarized light (below abbreviated as "width" and "PPL," respectively); b) dark component with significant proportion of dark groundmass. Larger dark patches are metal/sulfide. Note the thin, black vein cutting across the upper part of the image. Width: 5.5 mm, PPL; c and d) back-scattered electron (BSE) images of two melt pods in the leucocratic (c) and dark (d) phases. Note the angular geometries of these cross-sections through melt veinlets. Evidence for the presence of melt, e.g., in the form of tiny droplets of FeNi metal. Scale bars = 10 μm; e) a variety of chondrule types in the light component, including a compound chondrule (upper right) and a fractured and locally brecciated chondrule (lower middle). All dark blebs represent metal/sulfide. Width: 1.4 mm, PPL.

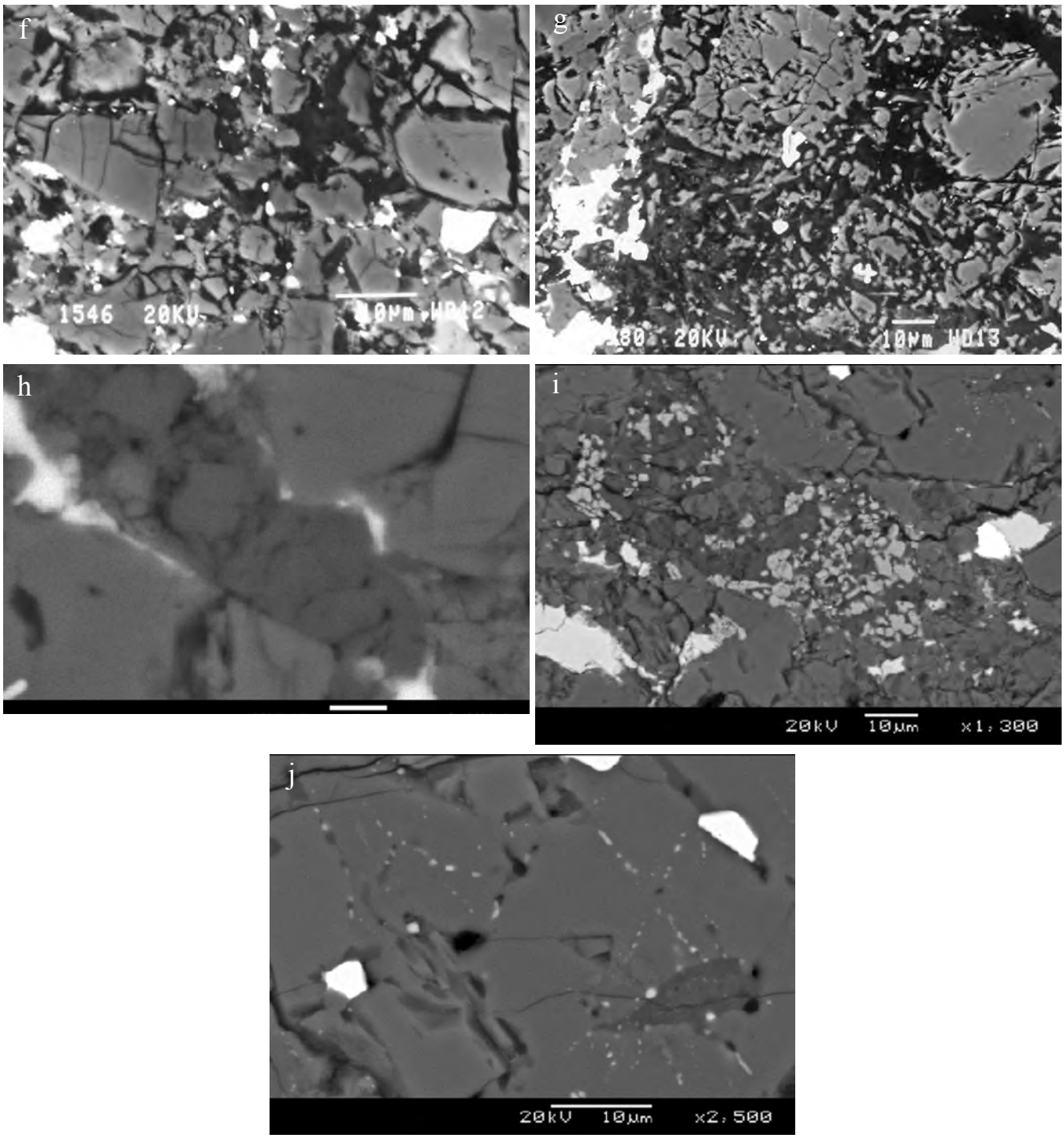

Fig. 3. *Continued.* Optical microscopic and SEM images taken on thin sections of sample #61: f–j): BSE images; f) groundmass of dark component with much feldspathic matrix (dark); note extensive fracturing and brecciation of silicate minerals. Scale bar = 10 μm; g) dark component—an area with even more feldspathic matrix. Slight variations in dark grey appearance of the matrix could be related to variable composition (variable K contents). Scale bar = 10 μm; h) brecciated feldspathic groundmass in dark component. The bright mineral is troilite. Scale bar = 2 μm; i) numerous chromite crystals associated with a pocket of feldspathic matrix in dark component. Note the central area with brecciated olivine (light grey). Scale bar = 10 μm; j) trails of troilite blebs forming planar to irregular alignments in olivine of the dark component. The dark area (right) is feldspathic melt with troilite droplets—a likely cross section of a thin melt vein. Scale bar = 10 μm.

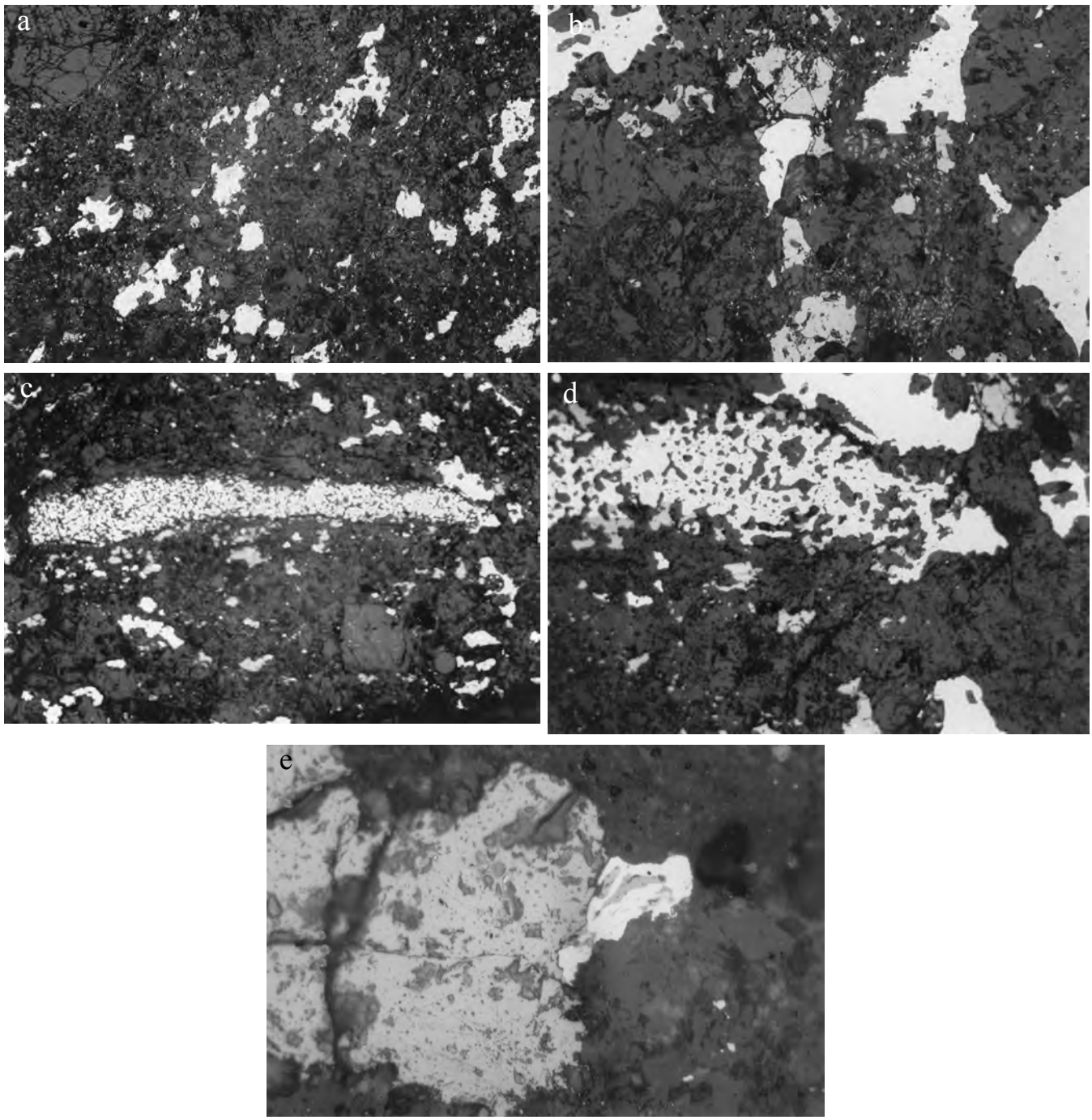

Fig. 4. Some impressions of metal/sulfide textures (4a, 4c, 4d, and 4e from sample 61, 4b from sample 58). All images taken in reflected light: a) disseminated FeNi metal and sulfide in different textural relationships (individual particles, intergrowths) within obviously brecciated (porous appearance due to high abundance of fractures) groundmass of dark phase. Note the highly varied shapes of metal and sulfide particles that attest to both recrystallization (thermal overprint) and deformation (brecciation, shearing). Width: 5.5 mm; b) evidence of brecciation in dark phase. Both sulfide and chromite (grey, angular fragments) display brittle deformation. FeNi metal is far more resilient against brittle deformation. The tiny, angular chromite particles occur in feldspathic melt pockets. Some of these angular particles are euhedral crystals, but others—at high magnification—belong together and represent the products of brecciation. Width: 0.7 mm; c) nearly 5 mm-long aggregate of FeNi metal and sulfide enclosing small areas of silicate minerals. Width: 5.5 mm; d) enlargement of a portion of the particle shown in Fig. 7c, emphasizing the spongy texture of this agglomerate and the relationship between FeNi metal and troilite surrounding the metal. Width: 0.7 mm; e) sulfide between FeNi metal as a result of shear (compare text for discussion). Width: 280 μm.

Table 3. Silicate mineral analyses. Data in wt%.

	Olivine	1 sigma		Opx	1 sigma	Selected Cpx analyses						
	n = 108			n = 94		1	2	3	4	5	6	7
SiO_2	39.3	0.6		56.3	0.8	55.6	54.2	54.4	56.9	54.2	55.0	55.2
TiO_2	0.02	0.03		0.15	0.08	0.17	0.14	0.19	0.22	0.39	0.57	0.04
Al_2O_3	0.02	0.08		0.23	0.19	0.29	0.87	0.42	0.31	0.51	0.73	0.22
Cr_2O_3	0.04	0.08		0.16	0.10	0.54	1.83	0.39	0.28	0.50	0.63	0.60
FeO	16.0	0.8		10.4	0.8	9.37	8.74	6.67	8.13	9.59	6.18	3.20
MgO	43.7	0.5		31.6	0.6	30.1	26.0	23.0	26.3	23.1	24.9	17.3
MnO	0.44	0.03		0.48	0.04	0.47	0.34	0.31	0.39	0.30	0.33	0.23
CaO	0.01	0.02		0.50	0.11	3.47	6.30	13.5	8.17	11.2	11.2	23.3
Na_2O	0.01	0.04		0.03	0.06	0.80	0.30	0.33	0.20	0.34	0.28	0.37
K_2O	b.d.	–		0.01	0.01	b.d.	0.03	b.d.	0.01	0.02	b.d.	0.01
Total	99.5	–		99.9	–	100.8	98.8	99.2	100.9	100.2	99.8	100.5
Fo	82.9	0.8	Wo	0.96	0.22	6.60	12.8	26.6	16.0	22.1	22.1	46.7
Fa	17.1	0.8	En	83.6	1.1	79.5	73.4	63.1	71.6	63.2	68.4	48.3
			Fs	15.5	1.1	13.9	13.8	10.3	12.4	14.7	9.52	5.01

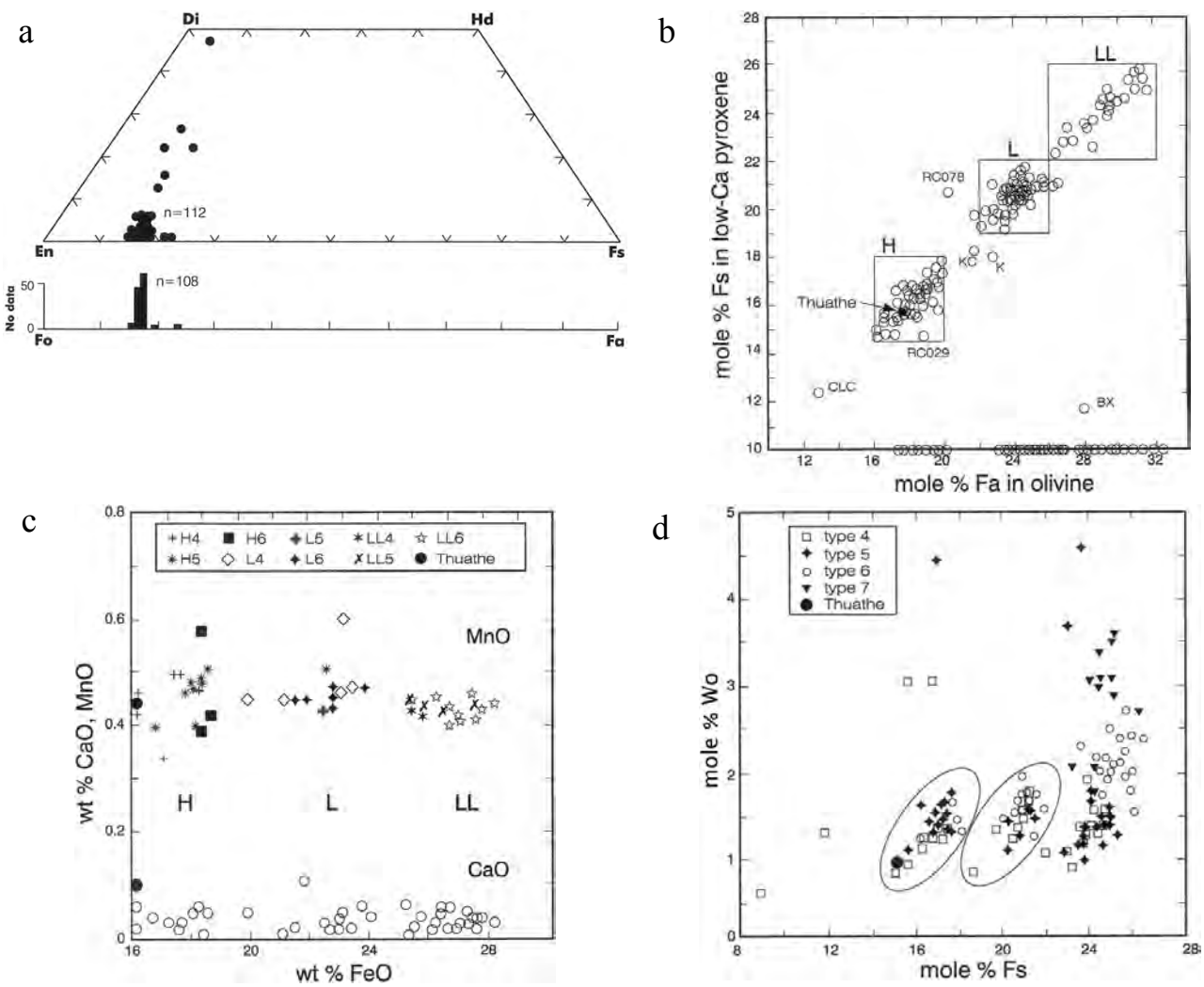

Fig. 5. a) Electron microprobe analytical results for olivine and pyroxene in Thuathe samples; b) mol% Fs in orthopyroxene versus mol% Fa in olivine from ordinary chondrites of different groups (after Brearley and Jones 1998, their Fig. 181). Thuathe data plot into the field for H-group chondrites; c) abundances of FeO and minor elements CaO and MnO in olivine of different groups and petrologic types of ordinary chondrites (after Brearley and Jones 1998, their Fig. 182) in comparison with Thuathe data; d) compositions of orthopyroxene in different groups and petrologic types of ordinary chondrites (after Brearley and Jones 1998, their Fig. 184).

Table 4. Kamacite, taenite, and troilite analyses. Data in wt%.

Kamacite (n = 112)				
	Min.	Max.	Mean	1 sigma
Mg	b.d.	0.15	0.02	0.01
S	b.d.	0.02	b.d.	b.d.
Cr	b.d.	0.19	0.01	0.03
Fe	88.0	95.4	92.8	0.8
Co	0.33	0.67	0.62	0.04
Ni	3.65	9.97	6.03	0.55
Cu	b.d.	0.07	0.01	0.02
Pb	b.d.	1.50	0.37	0.36
Total			99.9	
Taenite or taenite + kamacite (n = 16)				
	Min	Max.	Mean	1 sigma
Mg	b.d.	0.05	0.02	0.02
S	b.d.	0.03	0.01	0.01
Cr	b.d.	0.3	0.04	0.08
Fe	46.1	85.2	66.3	8.8
Co	0.14	0.29	0.24	0.04
Ni	14.5	53.7	32.7	9.0
Cu	0.03	0.35	0.21	0.07
Pb	b.d.	1.04	0.46	0.33
Total			100	
Troilite (n = 36)				
	Min.	Max.	Mean	1 sigma
Mg	b.d.	0.05	0.01	0.01
S	35.3	36.4	36.0	0.2
Cr	b.d.	0.50	0.03	0.08
Fe	61.5	62.9	62.2	0.3
Co	0.07	0.14	0.11	0.01
Ni	b.d.	0.17	0.01	0.03
Cu	b.d.	0.11	0.02	0.02
Pb	b.d.	1.30	0.52	0.39
Total			98.8	

Petrologic Type

As stated, olivine and orthopyroxene are well-equilibrated. In addition, feldspar is mostly fine-grained (<5 μm in size and confined to groundmass). The originally glassy groundmass of the chondrules is completely crystallized, and the outlines of chondrules predominantly are very distinct. Based on these analytical results and observations, the petrologic type of this new meteorite is 4 to 5 (see also Ambrose et al. 2003; Lombard et al. 2003). Our mineral chemical data do not allow unambiguous assignment to either of these groups. Also, even type 3 or 6 textures have been noted locally (R. Herd, personal communication: ". . . olivine crystallites . . . are typical of the finely preserved textures in type 4 OCs, or even in type 3, while the plagioclase-chromite ± phosphate intergrowths may be texturally indicative of a type 6 heating/recrystallization event").

Shock Metamorphism

With the exception of a few olivine grains that exhibit distinct, densely-spaced shock fracturing, only undulatory extinction has been noted in other crystals of this mineral. No other characteristic shock effects appear in the major silicate minerals. The shock pressure level for these deformations is less than 10 GPa. In addition, black veining has been noted in many specimens of Thuathe. On the basis of these observations, the shock metamorphic degree of this new meteorite is assigned to S2 to 3, according to Stöffler et al. (1991). Macroscopically, the meteorite represents a mixture of leucocratic clasts in relatively darker groundmass.

Veining

Up to 1 mm wide, but often thinner, black veins (Fig. 7) cut across many specimens. They are visible on the outsides of some stones but, in thin section, are quite abundant (Table 2). Generally, these veinlets are only several tens of μm wide. They frequently display a pinch-and-swell geometry (e.g., Figs. 7b and 7c). Displacement of sheared metal or sulfide grains is commonly noted along these veinlets (Figs. 7a–7c), with sulfide grains more often smeared out along a vein and dismembered into schlieren and/or droplets. Also, extensional fracturing has been induced along the veinlets, with many of these fissures having been filled by mobilized sulfide or metal (Fig. 7c). The geometries of these fractures are complex and suggestive of vein systems with multiple sets of extensional fractures related to different veins. Locally, distinct breccia (Fig. 7d) textures are the result. Besides these extensional fractures, injections of melt from clearly defined generation planes, up to >1 mm into the host, are noted and are distinguished by the presence of metal and/or sulfide droplets far from the loci of the likely precursor grains. Detailed high-magnification optical and SEM analysis showed that some veins vary in being locally characterized by either melting or brittle deformation only. This indicates that strain distribution along such fractures/veins was highly heterogeneous. It appears that melting along such microfaults (displacements are the rule) was facilitated where sulfide grains were encountered by the growing fracture. The geometries of offshoots are often straight, but some are irregular and meandering around larger entities (large olivine, metal/sulfide grains or chondrules). These offshoots exploit extensional fractures generated at the same time as the main generation plane. The SEM image in Fig. 8d shows a series of short offshoots from one of these veins that trend perpendicular away from the vein. Some offshoots are kinked, and the direction of these deviations is generally the same; it could indicate a movement direction along this vein.

Deformation veins were also investigated with the SEM. Figure 8a is a BSE image of a portion of such a vein between displaced parts of a troilite particle. The numerous droplets and schlieren of metallic material all represent, in this case, troilite melt. Late open fractures (micro-joints) cut across and displace this vein (and others). To the right of this area, the same vein was found to comprise a filling of angular

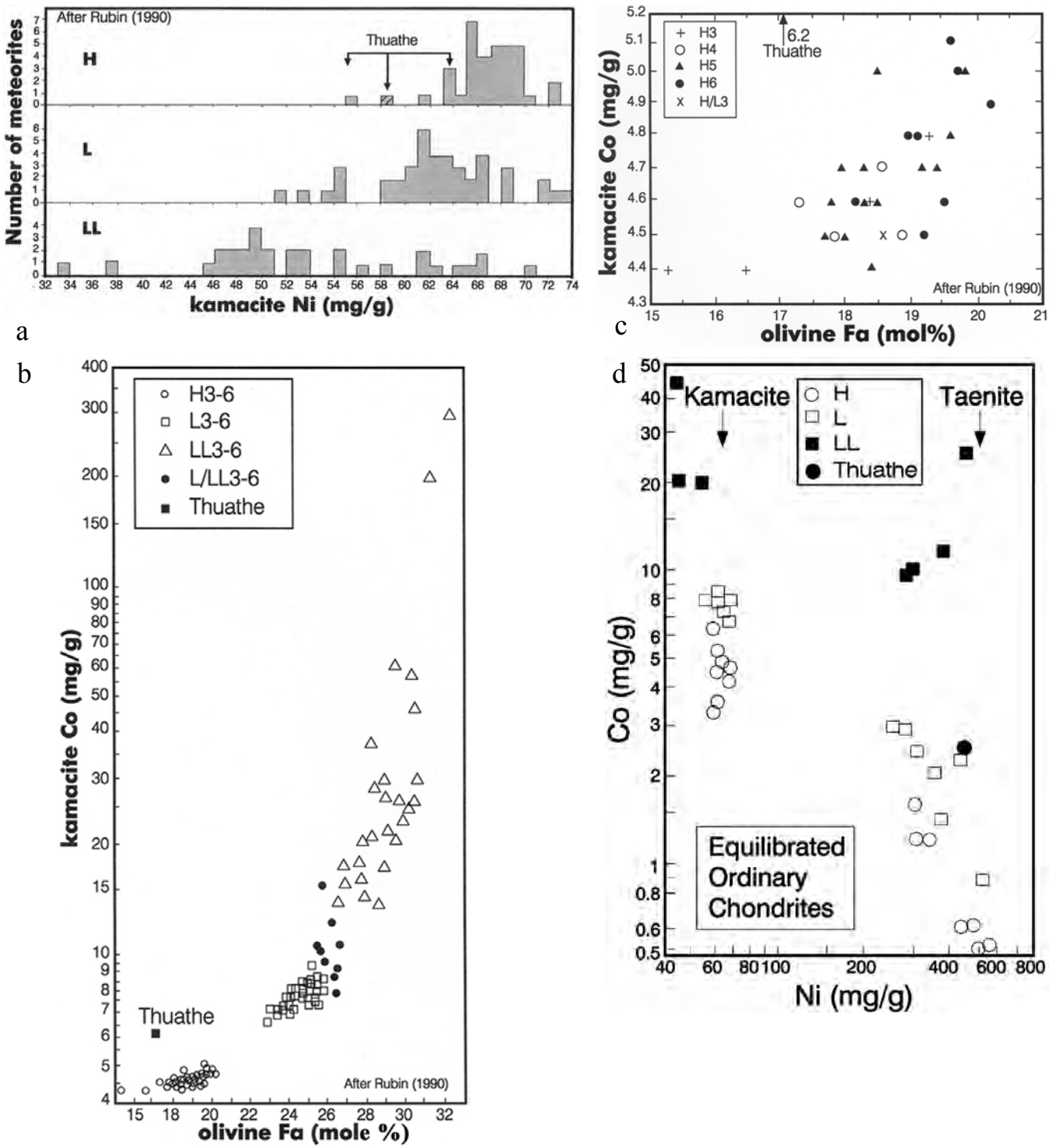

Fig. 6. a) Comparison of Ni contents in kamacite of various chondrite groups. Thuathe data overlap with the literature data (after Rubin 1990) for some H-group chondrites (lower range of spread for this group) and L group chondrites, thus, not permitting a definitive classification of Thuathe (hatched block: mean for the range of data that is indicated by the side arrows); b) comparison of Fa mol% and Co abundance in kamacite, for olivine and FeNi metal in different groups of ordinary chondrites (after Rubin 1990); c) comparison of olivine and kamacite compositions of Thuathe data with those for different petrologic types of H-group chondrites (after Rubin 1990); d) Ni and Co abundances in kamacite (left) and taenite (right) in Thuathe (individual data can not be distinguished at this scale) and other ordinary chondrites (literature data from Brearley and Jones [1998], after Afiattalab and Wasson [1980]).

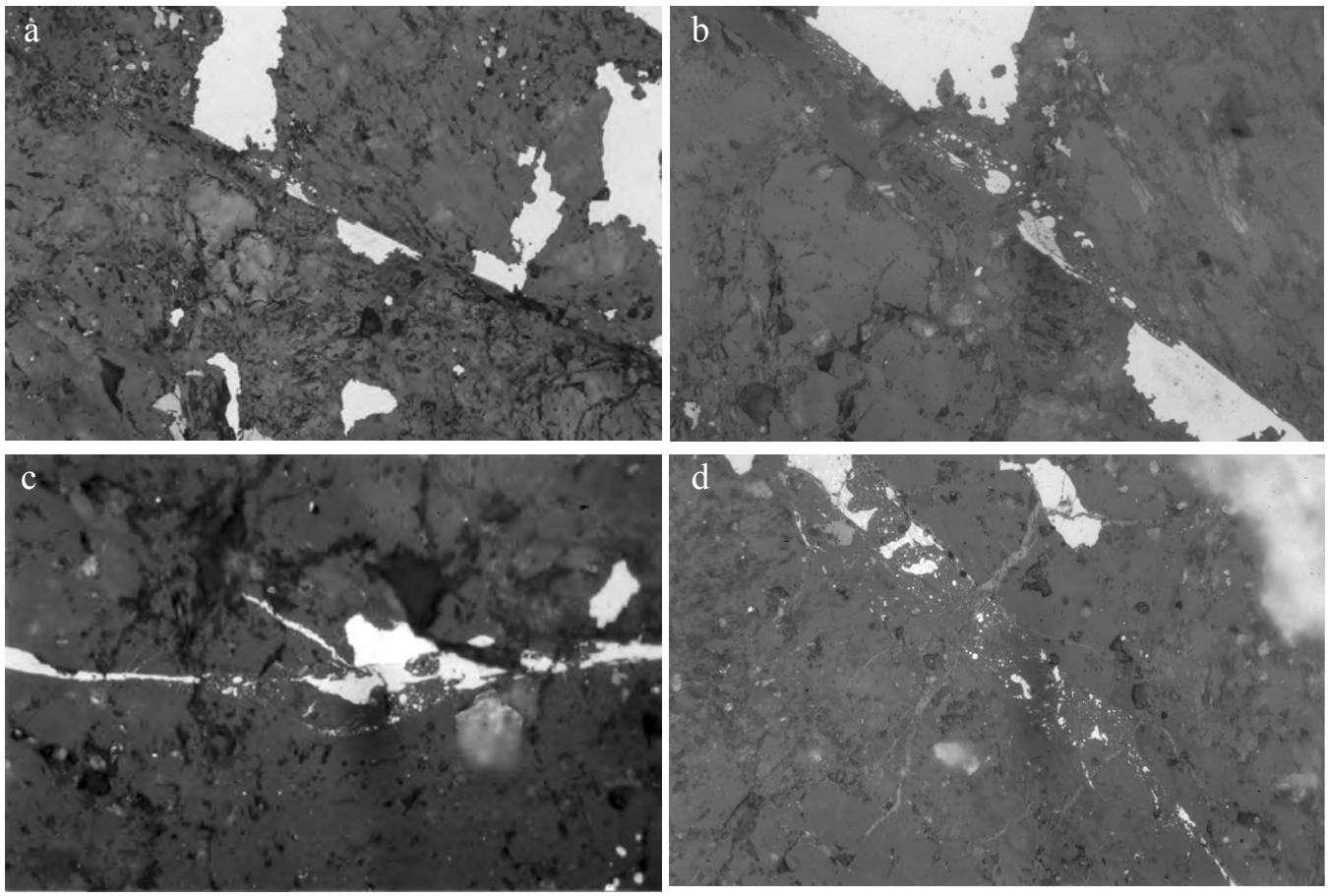

Fig. 7. Reflected light photography of narrow deformation veinlets (images 7a–7c from specimen 61, 7d from sample 58): a) sheared FeNi metal and sulfide grains alongside a veinlet. The precursor FeNi metal grain has been fractured and displaced but also locally melted (compare Fig. 7b). A troilite particle that existed at the rupture has been partially melted and plastically deformed (smeared out) along the vein. Width: 1.4 mm; b) enlargement of portion of previous image, illustrating the metal and sulfide droplets in the melt pocket developed between the two displaced FeNi metal grains. Width: 280 μm; c) a portion along another veinlet, where melting has affected only troilite. Note the extension fracture on the upper side of the veinlet that has been filled with mobilized sulfide melt; d) this portion of a deformation veinlet represents a melt breccia. Droplets of sulfide melt and irregularly shaped fragments of sulfide and/or FeNi metal occur in a silicate-dominated melt matrix. Parallel to the upper left portion of the vein, another curved off-shoot is noted that resembles the off-shoot separating a rip-off clast described in Fig. 7c. Note the grey veinlets cut by the breccia zone. They consist of Ni-poor Fe-oxide and are assumed to be a result of weathering in the wet environment after the fall. Width: 280 μm.

fragments of host silicate minerals only (Figs. 8b and 8c). The compositions obtained in the vein matrix range from pure troilite or kamacite to various mixtures of troilite and FeNi metal. Some grains also showed small abundances of Ca and P, presumably derived from melted phosphate, or Ca and Al, presumably derived from melted plagioclase. Silicate matrix analyzed in such veins yielded widely variable compositions, though they were generally dominated by Si, Mg, and Fe (after olivine and/or pyroxene). Always minor S, Ni, and/or P, Cr, and K were detected, demonstrating that the matrices are heterogeneous on a ten micrometer scale and were formed from melting of different local mineral assemblages. This supports an origin by friction, whereby melts of different minerals were mixed on a very small scale.

Importantly, the areas immediately adjacent to Thuathe veinlets are not characterized by an increase of deformation as known from many other chondrites where, for example, the presence of ringwoodite, majorite, or hollandite, or a shift from planar fracturing and undulatory extinction in olivine to mosaicism in the immediate environs of veins justifies the term “shock veining.” In the case of Thuathe, we cannot apply this term; our observations clearly favor a low-pressure fracturing process.

CHEMICAL COMPOSITION

Chemical Analysis

Major and trace element abundances of selected samples were analyzed by X-ray fluorescence spectrometry (XRF) and inductively coupled plasma mass spectrometry (ICP-OES) at Setpoint Laboratories in Johannesburg and by

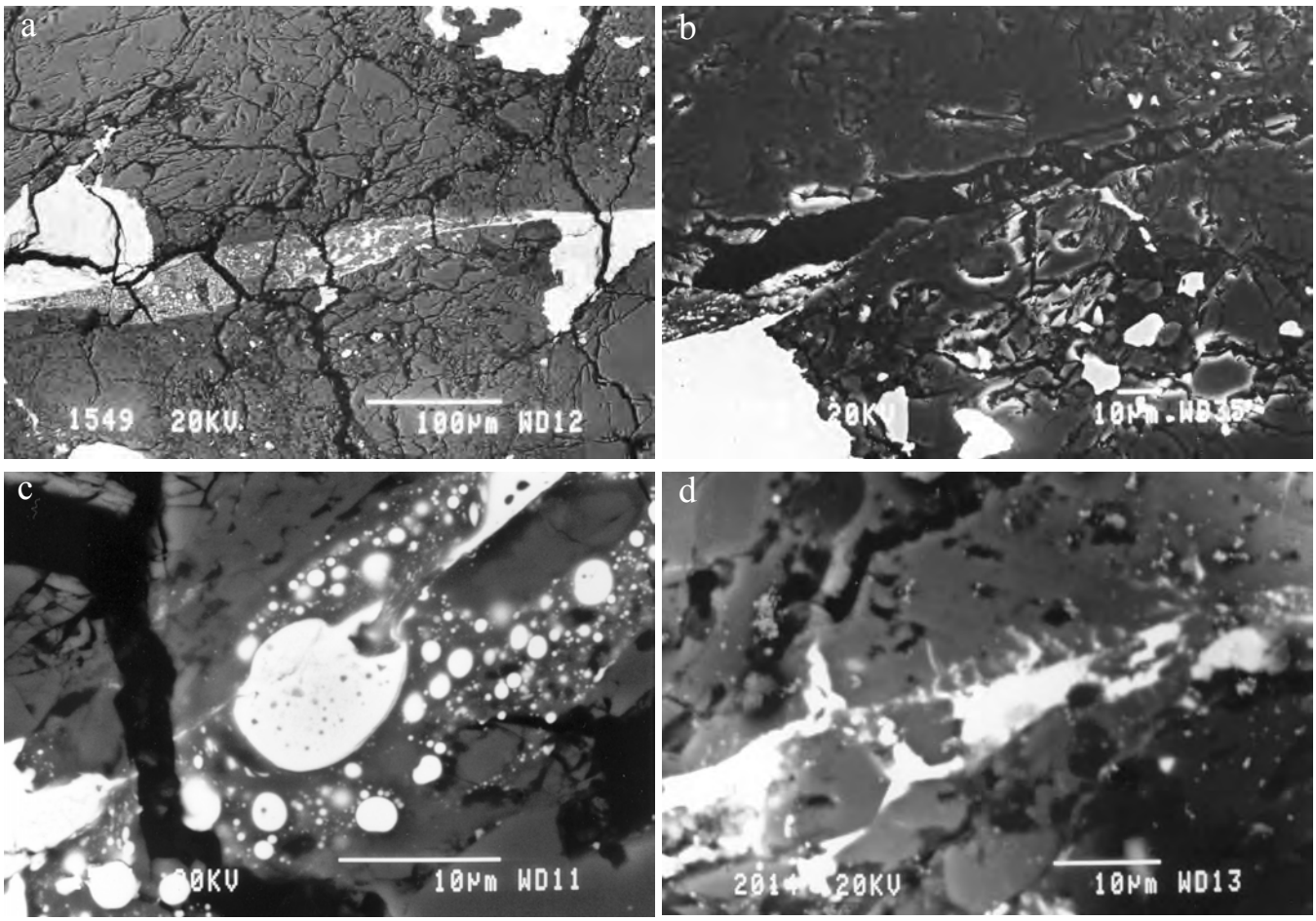

Fig. 8. SEM images of dark veinlets (images 8a–8c from sample 61, 8d from sample 58): a) a portion of a narrow dark vein between displaced troilite (note that the grain on the right is a composite particle also comprising some kamacite). No evidence for incorporation of FeNi metal into melt was detected. Scale bar = 100 μm; b) the same vein as in Fig. 8a but several mm to the right of the area shown in that figure. Only the products of brittle deformation (brecciation of olivine) are visible. Scale bar = 10 μm; c) numerous sulfide particles (with varied amounts of FeNi metal-derived component, compare text) in silicate-dominated matrix in a veinlet. See text for discussion of compositions of droplets and matrix. Scale bar = 10 μm; d) another vein displaying off-shoots of mobilized FeNi metal. Scale bar = 10 μm.

instrumental neutron activation analysis (INAA) at the University of Vienna, respectively. Sample preparation involved careful crushing and grinding of meteorite chips in agate mortar and pestle. XRF analysis was carried out on an ARL 9800 XP spectrometer. Sample powders (~2 g) were fused in Spectroflux 105 (Li Tetraborate/Li Carbonate/La Oxide). In addition, pellets of 13 g sample powder were prepared with a 10% wax binder component. Calibration curves were established with a series of SARM (South African Bureau of Standards; Potts et al. 1992) rock standards. The precision values for XRF analysis are: Fe, ±0.2 wt%; Mn, ±0.04; Ti, ±0.05; Ca, K, and Na, ±0.02; P, ±0.4; Si, ±0.1; Al, ±0.3; and Mg, ±0.1 wt%. For ICP-OES analysis with a Liberty 220 spectrophotometer, a 0.25 g sample was fused with $LiBO_2$, the melt was dissolved in acid and diluted to 100 ml. The SARM 46 standard was used for calibration of results. Accuracies for major elements were calculated at: SiO_2, 0.8; Al_2O_3, 1.5; Fe_2O_3, 0.95; MgO, 0.95; CaO, 2.3; Na_2O, 0.1; K_2O, 3; MnO, 1; TiO_2, 0.1; and P_2O_5, 0.1 wt%. For selected samples (Table 5), Fe contents were also determined by titration analysis at a precision of ±0.2 wt%. Details of the INAA methodology (including measurements, standards, instrumentation, precision, and accuracy information) are described by Koeberl (1993).

Major Element Results

Major and trace element data are presented in Tables 5 and 6, in comparison with ICP-MS data from Lombard et al. (2003). Major element data reveal some heterogeneity between the samples analyzed by our group and Lombard et al. (2003). The main differences are noted for the most abundant elements Si, Fe, and Mg. Our Fe analyses by different methods demonstrate that the various subsamples analyzed individually record varied amounts of metallic/sulfide phases. The range of our results for Fe (Tables 5 and 6)

Table 5. Major element data (ICP-MS; S by LECO as SO_4^{2-}; Fe also by titration {. . .}) for Thuathe samples. Data in wt%. For comparison, results for two samples by Lombard et al. (2003) are also shown (M-A, M-B); FC = fusion crust. [. . .]—INAA results.

Element	M-A	M-B	58	58FC	61A	61B
TiO_2	0.09	0.1	0.1	0.1	0.1	0.1
SiO_2	34.3	34.9	35.7	35.7	35.1	35.9
Al_2O_3	1.9	1.97	1.98	1.93	1.93	1.89
FeO	33.5	32.7	38.2	37.1	38.3	35.3
				{35.1}	{32.8}	{27.9}
				[37.3]	[35.7]	[31.9]
MnO	0.3	0.3	0.28	0.28	0.28	0.27
MgO	21.9	22.4	19.7	19.1	19.1	19.6
CaO	1.53	1.61	1.51	1.47	1.43	1.47
Na_2O	0.82	0.66	0.94	0.92	0.89	0.92
				[0.78]	[0.83]	[0.78]
K_2O	0.09	0.09	0.16	0.14	0.13	0.11
				[0.09]	[0.06]	[0.10]
P_2O_5	0.24	0.25	0.32	0.32	0.27	0.32
Cr_2O_3	0.48	0.5	nd	[0.49]	[0.54]	[0.49]
NiO	1.94	1.77	nd	[2.02]	[2.27]	[2.25]
SO_2	5.59	5.78	6.21	nd	5.15	4.56
Totals[a]	100.68	103.03	105.1	97.06	102.68	100.44
Si	16.03	16.3	16.68	16.68	16.4	16.77
Al	1.005	1.042	1.048	1.021	1.021	1
Fe	26.01	25.39	29.71	28.87	29.78	27.4
Mn	0.22	0.23	0.22	0.22	0.22	0.21
Mg	13.22	13.5	11.88	11.52	11.52	11.82
Ca	1.09	1.15	1.08	1.05	1.02	1.05
Na	0.61	0.49	0.7	0.68	0.66	0.68
Cr	0.33	0.34	–	0.34	0.37	0.34
Mg/Si	0.825	0.828	0.712	0.691	0.702	0.705
Al/Si	0.063	0.064	0.063	0.061	0.062	0.06
Ca/Si	0.068	0.07	0.065	0.063	0.062	0.063
Fe/Mg	1.97	1.88	2.5	2.51	2.59	2.32
Cr/Mg	0.025	0.025	–	0.03	0.032	0.029
Mn/Mg	0.017	0.017	0.019	0.019	0.019	0.018
Na/Mg	0.046	0.036	0.059	0.059	0.057	0.058
Fe/Si	1.62	1.56	1.78	1.73	1.82	1.63

[a]Naturally >100 wt%, as all Fe reported as FeO and all Ni as NiO, but much of the Fe and Ni occur as FeNi metal and Fe as troilite.

contains several low values in comparison to other published H chondritic abundances. The S contents are also quite variable, in agreement with the variable modal proportion of Fe-sulfide. In comparison with literature data for H chondrites (such as Mason 1979), the available major element results for Thuathe fall generally into the overall range of analyses reported. In Table 5, various major element ratios are presented for samples analyzed by our group and Lombard et al. (2003), and in Fig. 9a, such ratios are compared with those of different groups of ordinary chondrites (also compare Kimura et al. [2002], their Table 5). Thuathe trace element results compare well with published data for H chondrites (Mason 1979; Palme et al. 1981). However, while our Ni data are more variable than the range of published analyses, they still fall generally into the overall range for H chondrites. In binary trace element plots, Thuathe data fall readily into the H-group field (e.g., Fig. 9b). Rare earth element patterns (Fig. 9c) are characteristically chondritic (e.g., Palme et al. 1981; Mason 1979) with only negligible deviation from chondritic composition. In this diagram, and in Table 6, no significant and systematic differences in elemental abundances between the whole rock samples and fusion crust samples are detected. Notably, the significant variability of Fe contents observed in our ICP-MS data is supported by our INAA data, and by the ICP-MS data of Lombard et al. (2003). Ir/Si ratios for Thuathe fall into the range 4 to 4.5, which is at the lower end of the range for published H chondrite values (e.g., Wasson 1974, 1982).

Oxygen Isotopes

Oxygen isotopic data were obtained for two Thuathe

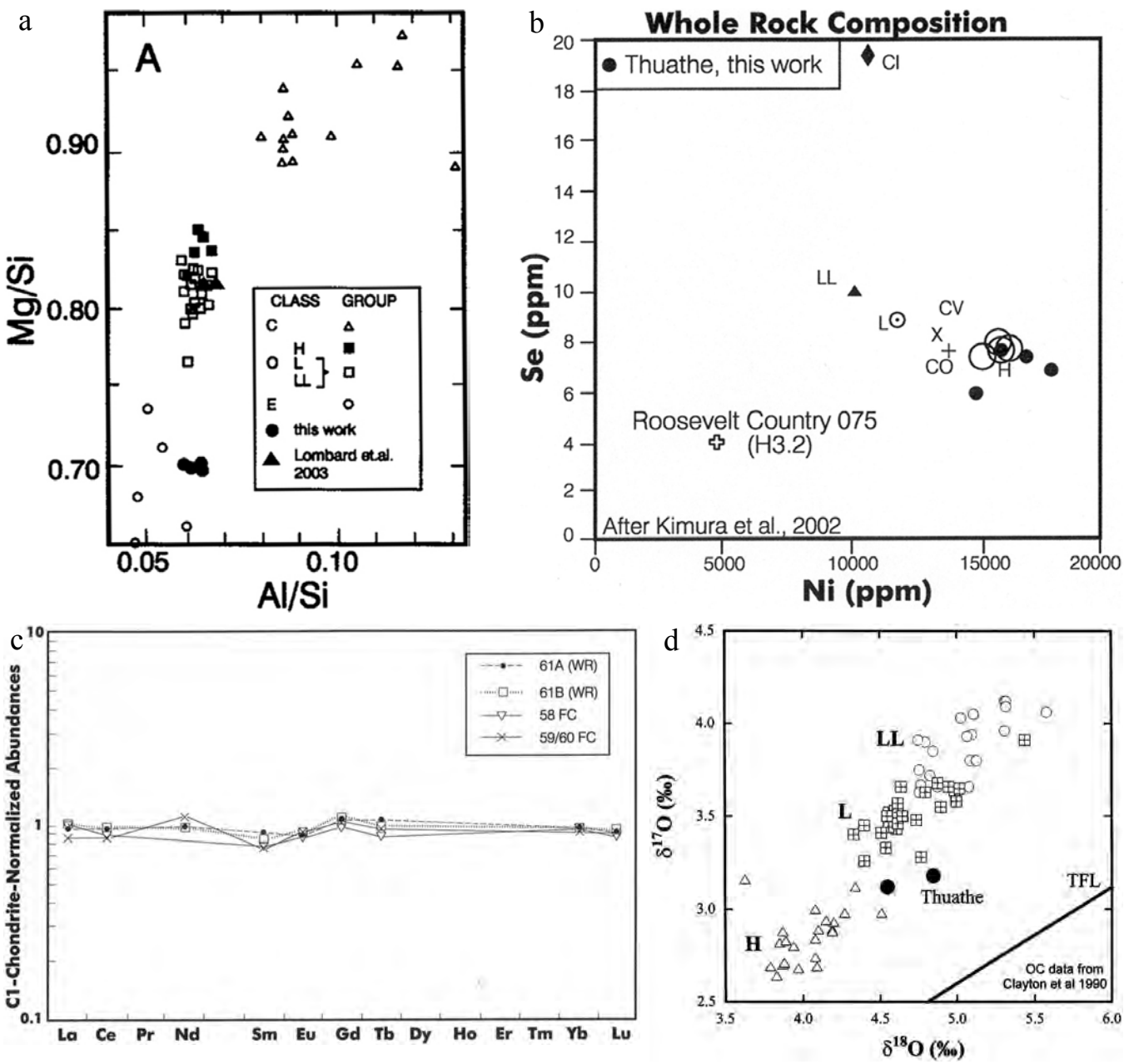

Fig. 9. a) Mg/Si versus Al/Si ratios for different groups of ordinary chondrites and Thuathe; b) Se versus Ni abundances for some ordinary chondrites (after Kimura et al. 2002) and Thuathe samples. Thuathe has distinct H-group affinity; c) CI-normalized (after Taylor and McLennan 1985) abundances of rare earth elements in four Thuathe samples, including two whole rock (WR; 61A and 61B) and two fusion crust (FC; from samples 58 and 59 + 60, respectively) specimens; d) oxygen isotopic composition of Thuathe samples (large filled circles). Also shown are the equilibrated ordinary chondrite data of Clayton et al. (1991) (open symbols) and recent high precision H chondrite data from Folco et al. (2004) (small filled circles). The terrestrial fractionation line (TFL) is shown for reference, and a mass fractionation line defined by data from Folco et al. (2004) is also indicated (HCFL).

samples by high precision laser fluorination at the Open University (U.K.). A small chip of sample 58 was crushed in an agate mortar and pestle, and two subsamples of 1.24 and 1.32 mg, respectively, were analyzed. The samples were heated with a CO_2 laser (10.6 μm) in the presence of BrF_5. The gases were purified with cryogenic (–196 °C) and KBr traps before being analyzed on a PRISM II (Micromass, UK) dual inlet mass spectrometer (for detail, see Miller et al. [1999]). The $\delta^{18}O$ value of the two aliquots of Thuathe were +4.55 and +4.85‰, with corresponding $\delta^{17}O$ values of +3.12 and +3.18‰ (compare Fig. 9d). The spread between the two data points is larger than normally expected for homogeneous samples, where typically ±0.02‰ is quoted for the uncertainty for $\Delta^{17}O$. This spread may reflect unexpected

Table 6. INAA data for Thuathe meteorite samples (this work), in comparison to Lombard et al. (2003)* ICP-MS results.

	61A	61B	58FC	59/60FC	Precision (rel%)	M-A*	M-B*
Na (wt%)	0.62	0.58	0.58	0.62	3	0.61	0.49
K	485	840	715	581	10	~750	~750
Sc	7.73	7.01	7.15	7.45	1	9.21	8.82
Cr	3710	3300	3340	3430	2	3285	3386
Fe (wt%)	27.8	24.8	29	24.2	5	26.01	25.39
Co	797	718	855	679	2	814	990
Ni (wt%)	1.78	1.77	1.59	1.48	10	1.53	1.39
Zn	23	36	34	35	5	61	59
As	2.12	2.03	2.58	1.98	3	1.66	2.62
Se	7.4	7	7.7	5.8	5	nd	nd
Br	0.28	0.11	0.15	0.15	5	nd	nd
Rb	5.1	5	4.5	4.1	5	2.6	2.5
Sr	<50	<30	<30	<30	–	11.5	11.03
Zr	10	8.9	8	9	20	5.75	5.42
Sb	0.077	0.051	0.061	0.11	10	nd	nd
Cs	0.049	0.1	0.029	0.07	15	nd	nd
Ba	<10	<10	<10	<10	–	4.13	3.82
La	0.35	0.37	0.38	0.32	–5	0.31	0.33
Ce	0.92	0.94	0.89	0.84	10	0.81	0.78
Nd	0.7	0.7	<1	0.8	15	0.56	0.55
Sm	0.21	0.2	0.19	0.18	5	0.18	0.73
Eu	0.076	0.081	0.079	0.082	5	0.07	0.06
Gd	0.33	0.34	0.31	0.32	20	0.24	0.24
Tb	0.062	0.058	0.053	0.056	5	0.045	0.043
Yb	0.24	0.24	0.25	0.23	5	0.21	0.2
Lu	0.035	0.036	0.037	0.035	10	0.034	0.032
Hf	0.1	0.12	0.13	0.14	10	0.15	0.15
Ta	<0.1	0.03	<0.1	0.03	–	0.04	0.05
Os (ppb)	805	720	740	685	10	nd	nd
Ir (ppb)	747	674	690	675	2	nd	nd
Au (ppb)	245	238	268	244	5	nd	nd
Th	0.05	<0.08	<0.06	0.05	10	0.05	0.05
U	0.02	<0.03	0.017	0.02	20	0.02	0.02
Ni/Co	22.3	24.7	18.6	21.8			
La/Sc	0.045	0.053	0.053	0.043			
Ir/Os	0.93	0.94	0.93	0.99			
LaN/YbN	0.99	1.04	1.03	0.94			
Eu/Eu*	0.88	0.95	0.99	1.04			

heterogeneity within the sample or an unrecognized analytical problem. Because this meteorite is a fall, significant weathering should not play a role; the sample analyzed for oxygen isotopes was from the interior of a 200 g specimen. Also shown in Fig. 9d are the data of Clayton et al. (1991) for equilibrated ordinary chondrites and more recent, high precision equilibrated H chondrite data from Folco et al. (2004) that were acquired by the same technique as the present data. The Thuathe results plot just outside of the normal field for H chondrites on an extension of a mass fractionation line of slope 0.52 defined by the high precision H chondrite data. The mean $\Delta^{17}O$ value of the H chondrites is defined as +0.77 ± 0.04 (Folco et al. 2004), and, therefore, the first of the Thuathe aliquots falls exactly on an extension of this mass fractionation line. The oxygen isotopic composition of Thuathe strongly indicates that this meteorite is an H chondrite, although the small shift to slightly higher $\delta^{18}O$ values suggests some differences from the vast bulk of equilibrated H chondrites, possibly reflecting differences in the metamorphic history or conditions, or even pre-metamorphic alteration history.

Noble Gases

Two bulk samples of Thuathe (#55 and 56; 105 and 110 mg, respectively) were analyzed using procedures given by Loeken et al. (1992). The uncertainties of concentrations are believed to be better than ±5 rel% for He, Ne, and Ar, but ±12 rel% for Kr and Xe, and those of isotope ratios are <1% except that of $^{129}Xe/^{132}Xe$, which should be <3%. For the calculation of exposure ages from the nuclides ^{3}He, ^{21}Ne, and ^{38}Ar, we used procedures and production rates described by

Eugster (1988). The results are given in Table 7; all calculated exposure ages are shown in Table 8. A U, Th-^{4}He gas retention age of 3.7 Ga is calculated with a U concentration of 13 ppb and a U/Th ratio of 3.6. The K-Ar age—calculated with a K concentration of 800 ppm—is 4.4 Ga.

Exposure Age and Shielding

The cosmogenic ^{22}Ne/^{21}Ne of Thuathe is 1.076, which indicates that these samples come from rather shielded positions of the meteoroid. Following Leya et al. (2000), the pre-atmospheric radius of this meteorite was >30 cm. The exposure age of Thuathe is 5 Ma, a low value compared to most other H chondrites, which show a prominent cluster around 7 Ma.

Cosmogenic Radionuclides

Specimen #57 was analyzed by non-destructive germanium gamma spectroscopy (Heusser et al. 1996) more than one year after the fall. The measured activity concentrations (in dpm/kd) are: ^{26}Al, 71.4 ± 5.4; ^{57}Co, 29 ± 11; ^{60}Co, 44.7 ± 3.8; ^{54}Mn, 138 ± 14; ^{22}Na, 99 ± 6. The uncertainties correspond to an 86% confidence level. Thuathe fell at a time when the galactic cosmic ray production rates were reduced against the averaged solar cycle level. A comparison of the normalized radionuclide concentrations (only ^{26}Al lives long enough so that the variations are averaged out) with model calculation for cosmogenic production rates in stony meteorites (see Leya et al. 2000, and references therein) shows that, for ^{26}Al, ^{22}Na, ^{57}Co, and ^{54}Mn, the maximum possible production rates have been reached in this sample. This is the case for the innermost parts of meteoroids with a radius >30 but <50 cm. The most sensitive depth indicator, ^{60}Co (Eberhardt et al. 1963), in combination with the others, indicates a pre-atmospheric radius of the meteoroid between 35 and 40 cm (corresponding to a mass between 620 and 930 kg), which is in good agreement with the above finding and the estimate based on the recovered mass. The primordial ^{40}K was also determined by this method at 1580 ± 60 dpm/kg, which corresponds to an abundance of 851 ppm K—in good agreement with the abundance obtained by chemical analysis (Table 6).

DISCUSSION AND CONCLUSIONS

Detailed observation and strong local interest resulted in detailed research of the fall of the Thuathe meteorite of July 21, 2002. This lead to a reasonable approximation of the path of the meteoroid shortly before its explosion and fall. The extent of the strewn field over the plateau and adjacent lowlands could be mapped and the distribution of finds within this area recorded. Mineral chemical studies, in particular the compositions of olivine and orthopyroxene, indicate that Thuathe should be classified as an H chondrite, especially on the basis of its olivine and pyroxene compositions. However, the FeNi metal phase is characterized by a slightly elevated (compared to other H chondrites) Co content. It is also evident from oxygen isotopes that Thuathe is not a common H chondrite. On the basis of well-equilibrated compositions of the main silicate phases (olivine and pyroxene) and textural observations (most feldspar grains in groundmass <4 μm in size; feldspathic groundmass in chondrules being completely recrystallized and the morphologies of chondrules generally well-preserved) but some inter-sample heterogeneity, this new meteorite is classified as predominantly of petrologic type 4 to 5.

Major element abundances for the samples analyzed in this study are variable and are in agreement with the mineralogical variation among the analyzed samples and, especially, with the variable contents of FeNi metal and sulfide. Thuathe is also of interest as it represents a brecciated meteorite composed of two phases—a dark component forming the groundmass to more leucocratic and partially ovoid to rounded clasts. While the mineral modes of the two components do not vary strongly, texturally, the dark component is quite different from the lighter material because of enhanced contents of feldspathic groundmass and relatively stronger brittle deformation of the silicate minerals.

Evidence of shock metamorphism is limited to some irregular fracturing and undulatory extinction in olivine. Only one olivine crystal with shock fractures characteristic for shock deformation below about 8 GPa was observed, and the overall degree of shock deformation observed does not exceed about 10 GPa. Consequently, the shock degree of Thuathe is classified as S2 to S3.

Table 7. Rare gas concentrations (in 10^{-8} cm^{3}STP/g) in Thuathe aliquots.

	^{3}He	^{4}He	^{20}Ne	^{21}Ne	^{22}Ne	^{36}Ar	^{38}Ar	^{40}Ar	^{84}Kr	^{132}Xe	^{129}Xe/^{132}Xe
Thuathe	7.47	1524	1.72	1.89	2.03	1.3	0.41	5620	0.018	0.031	1.38
	7.93	1552	1.54	1.84	1.98	1.4	0.5	5480	0.015	0.024	1.35
Mean	7.7	1538	1.63	1.86	2	1.35	0.45	6068	0.017	0.027	1.37

Table 8. Exposure ages and shielding parameter ^{22}Ne/^{21}Ne for Thuathe.

	^{22}Ne/^{21}Ne	Exposure Age (Ma)			
		^{3}He	^{21}Ne	^{38}Ar	Mean
Thuathe	1.076	4.8	4.7	5.2	4.9 ± 0.3

Both the light and dark components in Thuathe are cut by narrow deformation veins. These veins are in part composed of silicate and metal melts with the latter exsolved from the former in the form of droplets of various shapes. Local compositions in these veins are highly variable, but indicate that mixing occurred on a small scale. Other parts of these veins only show fracture fill that is the result of purely brittle deformation (cataclastic fill). Displacements of parts of crystals and grain aggregates along these veinlets is prominent and indicative of micro-faulting, while shearing is indicated by the plastic deformation of host grains at vein contents and clasts within veins. No increase of shock deformation is noted in the environs of such veins and in clasts within veins, in comparison to the overall low degree of shock metamorphism. Thus, it is concluded that these narrow deformation veinlets should not be called "shock veins" but, rather, are the product of faulting and shearing, with local strain enhancement having caused frictional melting. As silicates, including forsteritic olivine, have been melted along these deformation veinlets, temperatures upon vein formation must have been ~1500 °C locally. As with terrestrial pseudotachylitic breccia veinlets (Reimold 1995, 1998), different types of deformation veinlets ought to be distinguished in meteorites—those that are the result of shock melting (e.g., Walton and Spray 2003, and some references therein), possibly accompanied by frictional melting, and other veins that are purely the result of faulting, shearing, and friction only (also see van der Bogert et al. 2003). To categorize any dark veinlet as a "shock vein" is not adequate.

Thuathe experienced an interesting evolutionary history. In the early phase of this evolution, the macro-brecciation leading to the dark-light structure of this meteorite was generated. This was followed by strong thermal metamorphic equilibration. A first stage of vein formation followed and led to the development of the light grey, Fe >> Ni filled veinlets. At this time, we can only speculate as to whether this stage could be the cause of the slight differences in oxygen isotopic composition determined for two small aliquots of Thuathe. The light grey veining is, in turn, cut by the narrow black deformation veinlets recognized here as the result of faulting/shearing and local friction melting. Finally, perhaps in the meteorite fragmentation event associated with the fall in 2002, purely brittle micro-fracturing occurred.

Both the U, Th-^{4}He retention and the calculated K-Ar ages of 3.7 Ga and 4.4 Ga obtained from noble gas analysis, respectively, are typical for H chondrites and indicate that this meteorite was not involved in a major, late-stage thermal event. The concentrations of trapped heavy noble gases vary with their petrological type. The measured concentrations of ^{84}Kr and ^{132}Xe in two aliquots of Thuathe are in good agreement with type 4 (Loeken et al. 1992). Also, the measured ^{129}Xe/^{132}Xe of 1.37 is typical for that found in H chondrites. The calculated exposure age for Thuathe is 5 Ma, which is somewhat lower than the typical 7 Ma for H chondrites (compare, e.g., Marti and Graf 1992). Noble gas and cosmogenic nuclide analysis constrain the pre-atmospheric radius of the Thuathe meteoroid to 30–40 cm.

Acknowledgments–We are grateful to the many people living in the area of the strewn field who assisted with the evaluation of the fall and determination of the extent of the strewn field. Henja Czekanowska assisted with photography, Di du Toit and Lyn Whitfield with graphics, and Paula Ogilvie and staff of the Microanalytical Facility of the University of Pretoria with SEM work. R. Herd and A. Rubin are thanked for detailed reviews. Laboratory work by C. Koeberl is supported by the Austrian Science Foundation, project Y58-GEO. This is University of the Witwatersrand Impact Cratering Research Group Contribution No. 68.

Editorial Handling—Dr. Randy Korotev

REFERENCES

Afiattalab F. and Wasson J. T. 1980. Composition of the metal phases in ordinary chondrites: Implications regarding classification and metamorphism. *Geochimica et Cosmochimica Acta* 44:431–446.

Ambrose D. P. 2003. *Catalogue of stones from the strewn field of the Thuathe meteorite of 21 July 2002, 2nd ed.* House 9 Publications, Lesotho Miscellaneous Documents No. 8. Lesotho: Institute of Education, National University of Lesotho. 44 p.

Ambrose D. P. and Talukdar S. 2003. The day the stones fell from the sky. *Meteorite* 9(2):14–16.

Ambrose D. P., Reimold W. U. and Buchanan P. C. 2003. The Thuathe meteorite of 21 July 2002, Lesotho: Mapping the strewn field and initial mineralogical classification. *South African Journal of Science* 99:153–159.

Bevan A. and De Laeter J. 2002. *Meteorites—A journey through space and time.* Washington D.C.: Smithsonian Institution Press. 215 p.

Brearley A. J. and Jones R. H. 1998. Chondritic meteorites. In *Planetary materials,* edited by Papike J. J. Washington D.C.: Mineralogical Society of America. pp. 3-1–3-398.

Clayton R. N., Mayeda T. K., Goswami J. N., and Olsen E. J. 1991. Oxygen isotope studies of ordinary chondrites. *Geochimica et Cosmochimica Acta* 55:2317–2337.

Eberhardt P., Geiss J., and Lutz H. 1963. Neutrons in meteorites. In *Earth science and meteoritics,* edited by Geiss J. and Goldberg E. P. Amsterdam: North-Holland Publishing Co. pp. 143–169.

Eugster O. 1988. Cosmic ray production rates for ^{3}He, ^{21}Ne, ^{38}Ar, ^{83}Kr, and ^{126}Xe in chondrites based on ^{81}Kr-Kr ages. *Geochimica et Cosmochimica Acta* 52:1649–1662.

Folco L., Bland P. A., D'Orazio M., Franchi I. A., Kelley S. P., and Rocchi S. 2004. Extensive impact melting on the H chondrite parent asteroid during the cataclysmic bombardment of the early solar system: Evidence from the achondritic Dar al Gani 896. *Geochimica et Cosmochimica Acta* 68:2379–2397.

Heusser G., Ouyang Z., Oehm J., and Yi W. 1996. Aluminium-26, sodium-22, and cobalt-60 in two drill cores and some other samples of the Jilin chondrite. *Meteoritics & Planetary Science* 31:657–665.

Kimura M., Hiyagon H., Palme H., Spettel B., Wolf D., Clayton R. N., Mayeda T. K., Sato T., Suzuki A., and Kojima H. 2002. Yamato-792947, -793408, and -82038: The most primitive H

chondrites, with abundant refractory inclusions. *Meteoritics & Planetary Science* 37:1417–1434.

Koeberl C. 1993. Instrumental neutron activation análisis of geochemical and cosmochemical samples: A fast and reliable meted for small sample análisis. *Journal of Radioanalytical and Nuclear Chemistry* 168:47–60.

Leya I., Lange H. J., Neumann S., Wieler R., and Michel R. 2000. The production of cosmogenic nuclides in stony meteorites by galactic cosmic ray particles. *Meteoritics & Planetary Science* 35:259–286.

Loeken Th., Scherer P., Weber H., and Schultz L. 1992. Noble gases in eighteen stone meteorites. *Chemie der Erde* 52:249–259.

Lombard A., de Bruiyn H., Scholtz N., Praekelt H. E., Wilson A. H., and Schoch A. E. 2003. The Thuathe meteorite fall of 21 July 2002. *South African Journal of Science* 99:160–162.

Marti K. and Graf T. 1992. Cosmic ray exposure history of ordinary chondrites. *Annual Review of Earth and Planetary Sciences* 20: 221–243.

Mason B. 1979. Cosmochemistry. In *Data of geochemistry, 6th edition,* edited by Michael Fleischer. United States Geological Survey Profesional Paper 440-B-1. Washington D.C.: U.S. Government Printing Office. 132 p.

McKenzie R. S. 2003. Thuathe: A new meteorite from Lesotho. *Meteorite* 9(2):17–20.

Miller M. F., Franchi I. A., Sexton A. A., and Pillinger C. T. 1999. High precision $\delta^{17}O$ isotope measurements of oxygen from silicates and other oxides: Method and applications. *Rapid Communications in Mass Spectrometry* 13:1211–1217.

Palme H., Suess H., and Zeh H. D. 1981. Abundances of the elements in the solar system. In *Landolt-Börnstein: Numerical data and functional relationships in science and technology, vol. 2a.* Berlin: Springer-Verlag. pp. 257–272.

Potts P. J., Tindle A. G., and Webb P. C. 1992. *Geochemical reference material compositions.* Boca Raton: Whittles Publishing/CRC Press. 313 p.

Reimold W. U. 1995. Pseudotachylite—Generation by friction melting and shock brecciation? A review and discussion. *Earth-Science Reviews* 39:2470–264.

Reimold W. U. 1998. Exogenic and endogenic breccias: A discussion of major problematics. *Earth-Science Reviews* 43:25–47.

Reimold W. U., Buchanan P. C., Ambrose D., and Koeberl C. 2003. The H4/5 Thuathe meteorite fall of 21 July 2002, Lesotho: History of the fall, strewn field determination, and mineralogical and geochemical characterization (abstract). *Meteoritics & Planetary Science* 38:A15.

Rubin A. E. 1990. Kamacite and olivine in ordinary chondrites: Intergroup and intragroup relationships. *Geochimica et Cosmochimica Acta* 54:1217–1232.

Russell S. S., Zipfel J., Folco L., Jones R., Grady M. M., McCoy T., and Grossman J. N. 2003. The Meteoritical bulletin, No. 87. *Meteoritics and Planetary Science* 38:A189–A248.

Stöffler D., Kei K., and Scott E. R. D. 1991. Shock metamorphism of ordinary chondrites. *Geochimica et Cosmochimica Acta* 55: 3845–3867.

Taylor S. R. and McLennan S. M. 1985. *The continental crust: Its composition and evolution.* Oxford: Blackwell Publishing. 312 p.

van der Bogert C. H., Schultz P. H., and Spray J. G. 2003. Impact-induced frictional melting in ordinary chondrites: A mechanism for deformation, darkening, and vein formation. *Meteoritics & Planetary Science* 38:1521–1531.

Walton E. L. and Spray J. G. 2003. Mineralogy, microtexture, and composition of shock-induced melt pockets in the Los Angeles basaltic shergottite. *Meteoritics & Planetary Science* 38:1865–1875.

Wasson J. T. 1974. *Meteorites: Classification and properties.* Berlin: Springer-Verlag. 316 p.

Wasson J. T. 1982. *Meteorites: Their record of early solar system history.* New York: W. H. Freeman and Co. 267 p.